Scripta Materialia 163 (2019) 142–147

Contents lists available at ScienceDirect

Scripta Materialia

journal homepage: www.elsevier.com/locate/scriptamat

A novel composite-layered coating enabling self-enhancing thermal barrier performance

Guang-Rong Li [a], Li-Shuang Wang [b], Guan-Jun Yang [a,*]

[a] State Key Laboratory for Mechanical Behavior of Materials, School of Materials Science and Engineering, Xi'an Jiaotong University, Xi'an 710049, China
[b] School of Materials Science and Engineering, Xi'an Shiyou University, Xi'an 710065, China

ARTICLE INFO

Article history:
Received 16 October 2018
Received in revised form 6 January 2019
Accepted 10 January 2019
Available online 22 January 2019

Keywords:
Thermal barrier coating
Plasma spraying
Sintering
Thermal conductivity
Self-enhanced behavior

ABSTRACT

A novel composite-layered thermal barrier coating is designed to solve performance degradation caused by inevitable thermal exposure. Inspired by cathodic protection with a sacrificial anode, a degradation-resistant thermal barrier was achieved by the spontaneous formation of mesopores. The increment of thermal conductivity decreased from 110% for conventional coatings to 40% for composite coatings, which means 50% self-enhanced thermal insulation was realized. A new mechanism based on effective thermal-resistance was proposed to account for the self-enhanced behavior. The effective area for heat flux prevention was increased from 10 to 30% for 2D micropores to ~60% for the newly-formed 2D mesopores.

Thermal barrier coatings (TBCs) have been critical in enhancing the efficiency of modern propulsion and gas turbines related to energy-generation [1–6]. The primary function of TBCs is to enable the hot-sections to operate at temperatures higher than the limit temperature that the underlying metals can bear. The inlet temperature of a turbine can be increased by 100–300 °C when it is protected by a TBC with a thickness of 150–800 μm [7–9]. In addition, TBCs also need provide resistance to calcia-magnesia-alumino-silicate (CMAS) deposits during high-temperature operation [3,10–21]. Among various TBC fabrication technologies, the cost-effectiveness of atmospheric plasma spraying (APS) means that it continues to find wide application [15,22–25]. Moreover, the thermal conductivity of APS-TBCs is often <40% of that of the corresponding bulk material [26–29], compared to at least 60% for TBCs prepared by electron beam physical vapor deposition (EB-PVD) [30,31]. This enhanced thermal barrier performance is reached due to the lamellar structure of APS-TBCs, with inter-splat pores, intra-splat cracks, as well as globular voids [32]. The inter-splat pores, lying perpendicular to the heat flux, have a dominant role on the thermal barrier performance. Moreover, the in-plane lengths of the inter-splat pores are significantly larger than their out-plane widths [33]. Hence, they are hereafter called "two-dimensional (2D) micropores".

However, a key challenge for APS-TBCs is in retaining the excellent thermal barrier performance. TBCs operate at temperatures above 1000 °C, which causes sintering of the originally porous ceramic structure. As a result, the thermal conductivity of APS-TBCs can increase by 50–150% dependent on temperature and time, and hence the insulating capability would be sharply weakened [27,34–43]. For example, APS-TBCs made of yttria-stabilized zirconia (YSZ) have thermal conductivities of 1.0 $W \cdot m^{-1} K^{-1}$ in the as-deposited state, whereas this value increases to over 1.8 $W \cdot m^{-1} K^{-1}$ after thermal exposure at 1300 °C for 50 h [44]. This degradation is highly associated with the microstructural changes induced by sintering. The main structural change is the "healing" of 2D micropores. In situ and quantitative data suggest that approximately 50% of these pores are healed during thermal exposure [45–48]. Unfortunately, the sintering of ceramics at high temperatures, along with their trend to be densified, is inevitable. Therefore, how to realize sintering resistant ceramic coating at high temperature is key to achieving sustainable thermal barrier function during thermal service.

Our structural design is based on the widely known sacrificial anode protection [49–51]. In this method, the target metal (cathode) is protected from corrosion by sacrificially corroding another metal (anode). This suggests that two materials' differentially changing behaviors can be utilized to spontaneously resist degradation under a specific service environment. Inspired by this idea, a novel composite-layered structure is tailored to control the sintering effect during thermal exposure. Differential contractions of different layers can defy overall sintering, despite sintering of each respective region occurring. Consequently, overall sintering-resistant structure can be realized, which would essentially solve the problem of degradation caused by sintering. In this study, we highlighted the relationship between

* Corresponding author at: State Key Laboratory for Mechanical Behavior of Materials, School of Materials Science and Engineering, Xi'an Jiaotong University, Xi'an, Shaanxi 710049, China.
E-mail address: ygj@mail.xjtu.edu.cn (G.-J. Yang).

https://doi.org/10.1016/j.scriptamat.2019.01.010
1359-6462/

designed microstructure and thermal property, and investigated the underlying mechanism responsible for the degradation-resistant behavior.

A composite-layered structure is formed by alternatively stacking two kinds of splats. The first ones are resolidified from their molten states prepared by APS. In addition, these splats are further divided into several splat segments by intra-splat cracks. The limitation of minimum particle size in APS suggests that new approaches should be used to deposit sub-micrometric particles. Recently, suspension plasma spraying (SPS) and solution precursor plasma spraying (SPPS) are widely investigated [22,52–57]. The tailored coatings have low thermal conductivity and long lifetime [58–61], owing to the large quantity of micro and nanometer pores and segmented structure, respectively. The strain tolerant nature of SPPS can even be used to prepare durable TBCs with large thickness [62]. Therefore, the second ones are deposited by SPS to form nanopowder heaps. For comparison, conventional mono-layered coatings formed by APS are also prepared. Fig. 1 shows schematics of the stacking processes of the conventional and composite coatings; the supplementary file provides information about the sample preparation, structural characterization, and measurement of thermal properties.

Fig. 2 shows cross-sectional images of conventional and composite coatings during thermal exposure. In the as-deposited state, lamellar features can be clearly found in both coatings, confirming the fact that the coatings were formed by the stacking of individual splats [63–65]. The splats are often partially bonded together, leaving a large quantity of 2D micropores. These 2D micropores provide great insulation against thermal exposure, since they are oriented perpendicular to the heat flux.

During thermal exposure, evolution of the composite and conventional coatings can be divided into two stages (Fig. 2c), and the boundary is located at approximately 10 h. This two-stage evolutionary trend is consistent with previous reports [45,66]. In stage I, the trends of change of the coatings appear to be similar. The length density of 2D pores, defined as the total lengths of 2D pores in unit area, is decreased by approximately 50%. In stage II, the composite coating shows a contrasting trend compared to the conventional coating. In the conventional coating, the length density of the 2D pores continues to decrease, albeit at a much lower rate than that in stage I, whereas in the composite coatings, the length density of the 2D pores increases. Moreover, the polished cross-sections show that new pores are formed. These newly-formed pores clearly have a 2D morphology, but they are longer than the 2D micropores observed in the as-deposited state. Therefore, they are hereafter called “2D mesopores.” It is reported that the microstructure would evolve further under thermal and mechanical load, in order to relax stresses caused by stiffness [10,11,20,67–69]. And this is one of the reasons to form new pores or cracks. However, the samples used in this study are free-standing coatings. Therefore, the external loading effect may be not the main reason, since no obvious 2D mesopores can be found in conventional samples, as shown in Fig. 2 (a). In fact, a few of these mesopores are reminiscent of the original large pores, but most of them are resulted from the interfacial opening between splats formed through APS and through SPS, as shown in Fig. 2(f). On one hand, the contractions of the splats formed through APS and the neighboring splats formed through SPS can be totally opposite. On the other hand, the splats formed through SPS are actually loose nanopowder heaps, which undergoes a greater contraction degree than that of the splats formed through APS, since the nanopores significantly increase the surface energy [70]. These differential contractions result in the opening of the interface between these two different kinds of splats, thus forming 2D mesopores. This is similar to the nanostructured TBCs [71,72].

In fact, the sintering mechanisms of the splats formed by APS and by SPS are completely different. In a zone formed by APS, sintering occurs through the healing of the 2D micropores [66]. First, nanoscale roughening caused by thermal grooving at the grain boundaries and faceting at the grain surface is observed along the smooth surfaces of the 2D micropores. This roughening yields multiple contacts which bridge the facing surfaces [44,73]. This provides more paths for matter transfer (Fig. 2e), significantly accelerating the sintering process in stage I [45]. In contrast, regarding the nanopowder heaps, the sintering occurs through the healing of 3D nanopores. Only single contact is formed between two spherical nano-powders, which is similar to the powder metallurgy

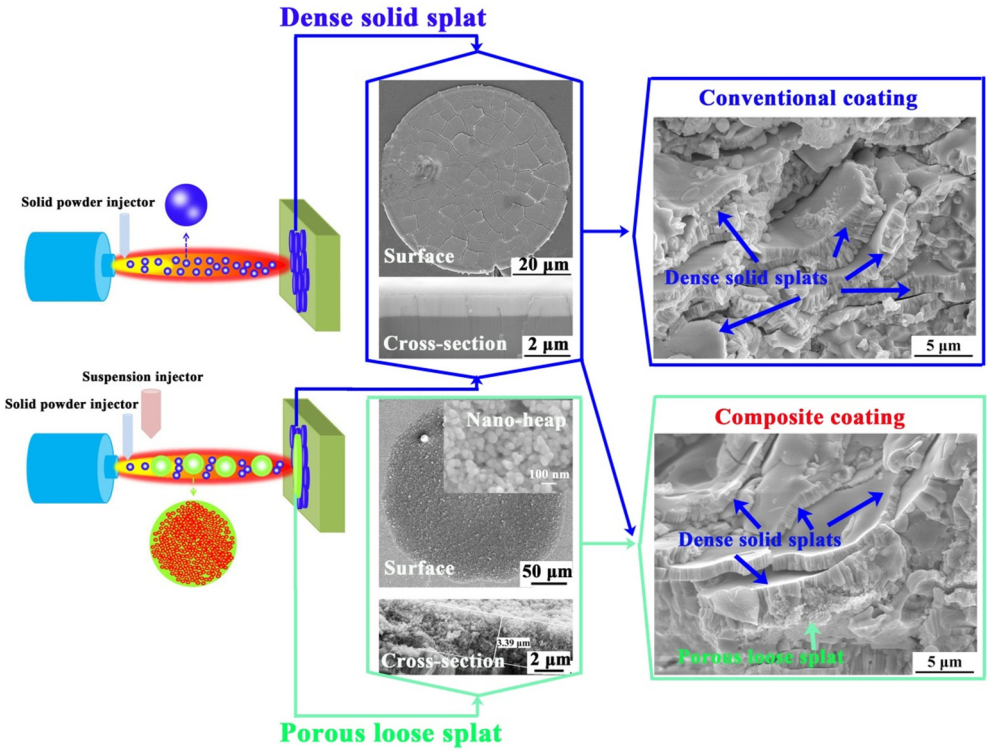

Fig. 1. Schematics of the stacking processes of conventional and composite coatings.

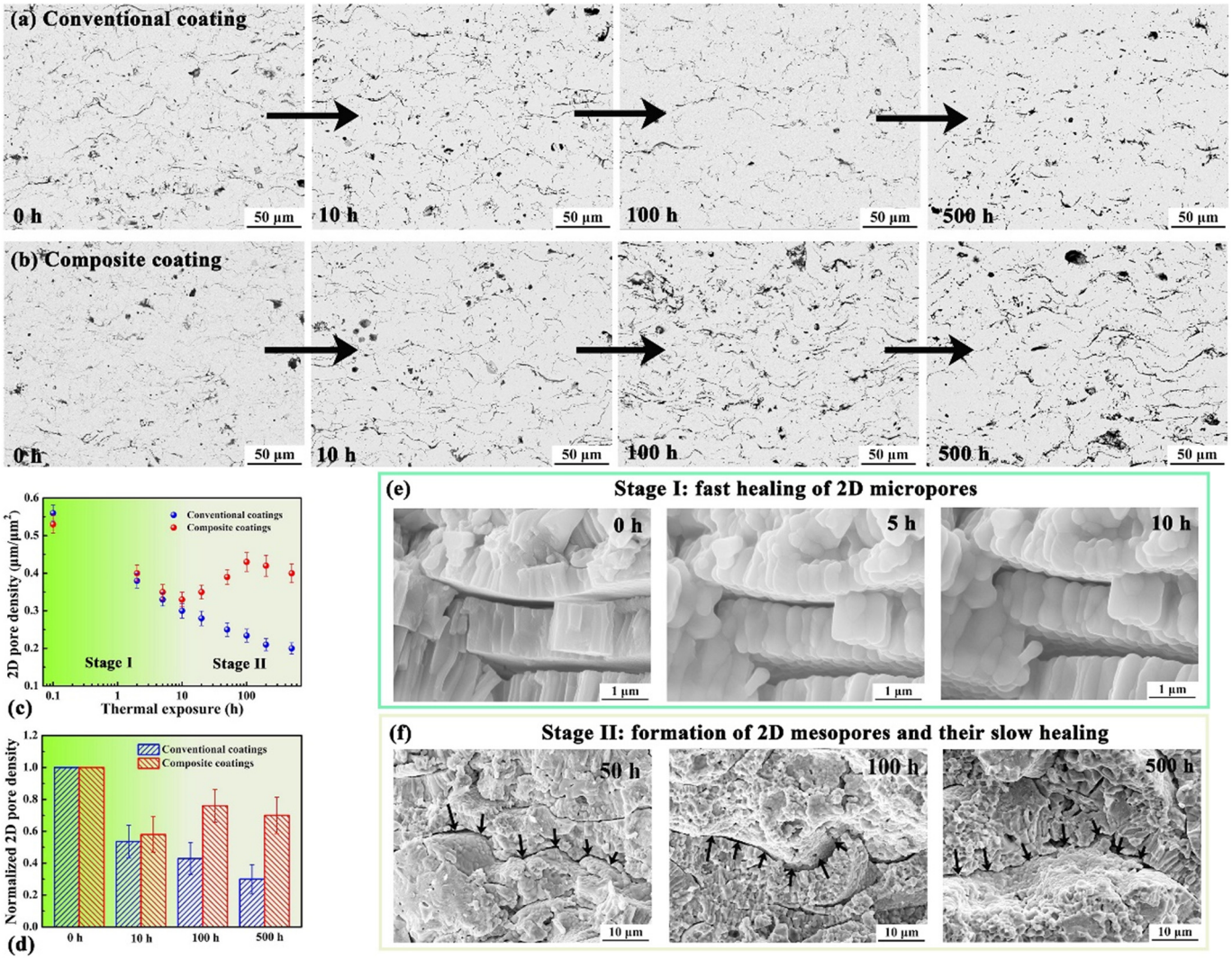

Fig. 2. Microstructural evolutions of conventional and composite coatings during thermal exposure: (a) polished cross-sections of conventional coatings, (b) polished cross-sections of composite coatings, (c) changes of 2D pore density, (d) normalized 2D pore density, (e) healing of 2D micropores between dense splats, and (f) formation of 2D mesopores.

[74]. During sintering, the diameters of the contacted necks grow, resulting in the gradual disappearance of the 3D nanopores.

Fig. 3 demonstrates how the thermal conductivities of the conventional and composite coatings were affected by the duration of thermal exposure. At as deposited states, the thermal conductivity of the composite coatings is slightly lower than that of the conventional coatings. The cause is that the splats deposited by SPS introduced some submicron and nanopores, which contribute mainly to the thermal barrier performance of the SPS and SPPS TBCs [53,60]. Moreover, the designed layered-SPPS coatings even have lower thermal conductivity compared with the APS coatings [54,75]. This novel layered-SPPS coating with excellent thermal insulation also inspired us to design the composite layered structure, so as to achieve optimized thermal barrier performance.

During thermal exposure, the thermal evolution can also be divided into two stages. For the conventional coating, stage I and stage II represent 80% and 120% increase in thermal conductivity, respectively. This

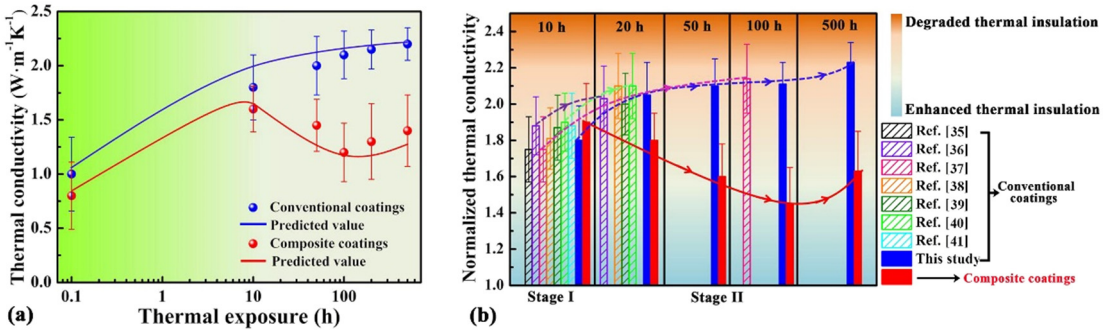

Fig. 3. Effect of thermal exposure on the thermal conductivities: (a) changes in thermal conductivities as a function of thermal exposure durations, and (b) normalized thermal conductivity at different stages with respect to the as-deposited state.

was similar to that cited in other reports [35–41], as shown in Fig. 3b. The degrees of increase are consistent in each stage for conventional coatings, which implies that the thermal insulation is degraded throughout the duration of thermal exposure. However, for the composite coatings, stage I and stage II represent 90% and 40% increase in thermal conductivity, respectively. This suggests that the thermal insulation is recovered in stage II to a significant degree. Moreover, this recovered thermal insulation can remain for long time. This is highly related to the healing mechanism of the 2D pores. The ultrafast sintering kinetic in stage I is mainly caused by accelerated matter transfer induced by the multiple contact points [45]. However, these multiple contact points are dependent on the roughening scale and the width of the 2D pores. It is reported that the roughening scale is about 30–50 nm, which is larger than the width of the 2D micropores (<20 nm) [66]. Therefore, significant healing of the 2D micropores occurs in stage I (Fig. 2). In contrast, the newly-formed mesoscale 2D pores often have a width larger than 50 nm, suggesting that they are relatively unable to be bridge-connected by roughening. This is consistent with a previous report [76], which proposed a critical healing width for ceramic coatings.

The changes in thermal conductivity can be correlated with the changes in 2D pore density. In stage I, the 2D micropores are healed significantly, which is highly consistent with the obvious increase in thermal conductivity. In stage II, the increase of thermal conductivity in the conventional coatings seems to be gradual, correlating to the slight healing of 2D micropores. In contrast, the decrease of thermal conductivity in the composite coatings is caused by the formation of 2D mesopores. A structural model was developed to predict thermal conductivity by quantitatively correlating the structural and thermal properties as a function of thermal exposure duration. In this model, the variable is the change of 2D pore length, including the 2D micropores and the newly-formed 2D mesopores. Other details about the structural model can be found in the supplementary material. The predicted changes of thermal conductivity are consistent with the experimental data. Therefore, the quantitative relationship between structure and properties suggests that the 2D pores of multiple scales dominantly determine the thermal properties.

The enhanced thermal insulative performance may be caused by two reasons. The first is the multiscale pores introduced by SPS. The coatings prepared by SPS often have large quantity of micron and submicron pores, which contribute to the overall low thermal conductivity [58–61]. The second is the newly-formed 2D mesopores. Fig. 4 shows the effect of pores with different aspect ratios on temperature distribution and heat flux. Just like the mesopores formed in the composite

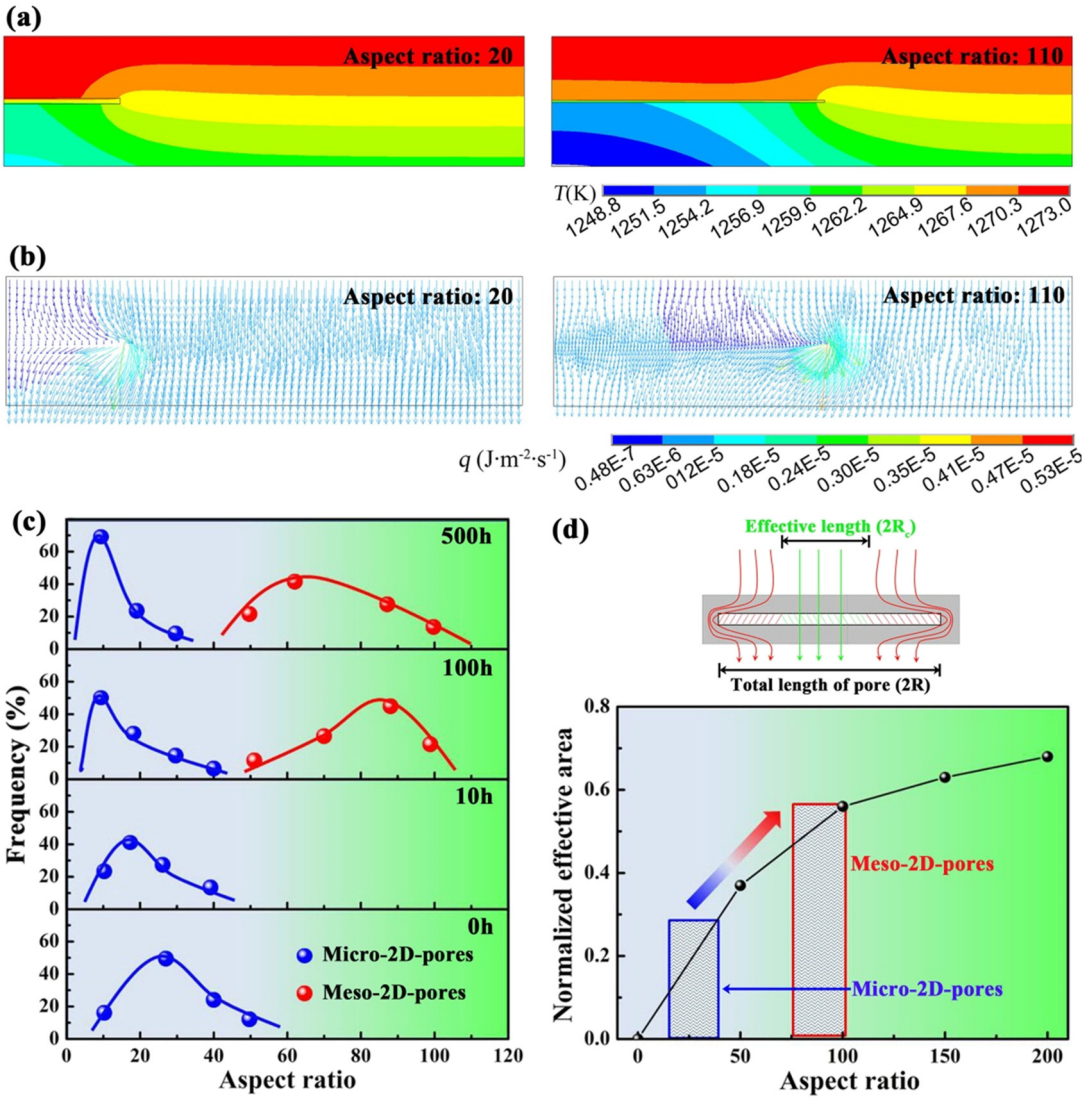

Fig. 4. Effect of pores with different aspect ratios on thermal barrier performance: (a) temperature distributions, (b) heat flux, (c) aspect ratios of 2D micropores and mesopores, and (d) normalized effective area as a function of aspect ratio of pores. In Fig. 4d, the blue and red columns represent the main ranges of aspect ratios of the 2D micropores (15–40) and the newly-formed 2D mesopores (75–100), respectively.

coatings, the pores are perpendicular to the heat flux. Based on Fig. 2, the mesopores appear to be obvious at stage II, in particular at 100 h. Therefore, we present the aspect ratios of mesopores at 100 h and 500 h. From the temperature distribution (Fig. 4a), it is found that pores contribute to a significantly higher temperature drop than solid material. Moreover, the highest temperature drop occurs at the pore center, and decreases gradually from the center to the edge of the pores. In fact, the pores result in a 2D heat flux distribution (Fig. 4b). At the center of pores, the heat flux is perpendicular to the pores, while that at the edge of pores is only somewhat affected. This means that the heat flux at the center of the pore passes through it, whereas that at the edge of the pore bypasses it. This phenomenon can also be found in other reports [77,78]. The thermal conductivities of the solid material and the air-trapped pores are 2.5 $W \cdot m^{-1} K^{-1}$ and 0.025 $W \cdot m^{-1} K^{-1}$, respectively. Therefore, the temperature drop decreases from the center to the edge of the pores. The method to determine the pattern of heat flux is described as follows: (i) the heat flux vector q is divided into q_x and q_y, which refer to the X-component and the Y-component of the heat flux vector q, respectively; (ii) the heat flux bypasses the pores if $|q_x| > |q_y|$, whereas the heat flux passes through the pores if $|q_x| < |q_y|$. The critical condition $|q_x| = |q_y|$ corresponds to a critical pore of radius R_c, as shown in Fig. 4d. The area within R_c of a pore would have effective thermal insulation against heat flux, defined as the "effective area." Fig. 4d shows the normalized effective area (πR_c^2) with respect to the total area (πR^2) as a function of the aspect ratio. Overall, the normalized effective area increases with the aspect ratio. The blue column represents the main range of aspect ratios of the 2D micropores, which is approximately 15–40 observed from Fig. 4(c) at 0 h. In previous reports [8,23,28,33,39], the aspect ratios of the 2D micropores are <50, and the corresponding normalized effective area is <30%. In contrast, the red column stands for the main range of aspect ratios of the newly-formed 2D mesopores, which is approximately 75–100 observed from Fig. 4(c) at 100 h. As a result, their normalized effective area increases to nearly 60%. That means the 2D mesopores are fully utilized in the prevention of heat flux. This is the main contribution of the 2D mesopores on the self-enhancing thermal insulation of the composite coatings.

In this study, a novel composite-layered coating was designed to solve the issues of TBC performance degradation caused by inevitable thermal exposure. 2D mesopores oriented against the heat flux were newly-formed during thermal exposure. The increment of thermal conductivity was decreased from 110% for conventional coatings to 40% for composite coatings, which means 50% self-enhanced thermal insulation was achieved. Quantitative analysis confirmed that the 2D pores of multiple scales dominantly determined the thermal insulation. A mechanism based on the effective thermal-resistance of 2D pores was proposed to account for the self-enhancing behavior. The effective pore area which for preventing heat flux increased from the conventional 10–30% to nearly 60% for the composite coatings. The novel design enables TBCs to retain high thermal barrier performance under thermal service environment, which will provide a fundamental contribution to the next generation of advanced TBCs.

Acknowledgments

This work was supported by the National Natural Science Foundation of China (grant number 51801148); the China Postdoctoral Science Foundation (grant number 2018M631151); the Equipment Advance Research Foundation (grant number 61409220117); the Shaanxi Province Postdoctoral Science Foundation; the Fundamental Research Funds for the Central Universities; and the National Program for Support of Top-notch Young Professionals.

Declarations of interest

None.

Appendix A. Supplementary data

Supplementary data to this article can be found online at https://doi.org/10.1016/j.scriptamat.2019.01.010.

References

[1] N.P. Padture, M. Gell, E.H. Jordan, Science 296 (5566) (2002) 280–284.
[2] N.P. Padture, Nat. Mater. 15 (8) (2016) 804–809.
[3] L.R. Turcer, N.P. Padture, Scr. Mater. 154 (2018) 111–117.
[4] J. Yang, Y. Han, M. Shahid, W. Pan, M. Zhao, W.J. Wu, C.L. Wan, Scr. Mater. 149 (2018) 49–52.
[5] Z.L. Qu, K. Wei, Q. He, R.J. He, Y.M. Pei, S.X. Wang, D.N. Fang, Ceram. Int. 44 (7) (2018) 7926–7929.
[6] Z.L. Qu, M.A. Yu, Y.C. Liu, B.S. Xu, R.J. He, Y.M. Pei, H.W. Zhao, D.N. Fang, Rev. Sci. Instrum. 88 (4) (2017), 045102-1-8. .
[7] D.R. Clarke, M. Oechsner, N.P. Padture, MRS Bull. 37 (10) (2012) 891–902.
[8] R. Vassen, A. Stuke, D. Stover, J. Therm. Spray Technol. 18 (2) (2009) 181–186.
[9] L. Chen, P. Song, J. Feng, Scr. Mater. 152 (2018) 117–121.
[10] A.R. Krause, H.F. Garces, C.E. Herrmann, N.P. Padture, J. Am. Ceram. Soc. 100 (7) (2017) 3175–3187.
[11] A.R. Krause, H.F. Garces, G. Dwivedi, A.L. Ortiz, S. Sampath, N.P. Padture, Acta Mater. 105 (2016) 355–366.
[12] A.R. Krause, X. Li, N.P. Padture, Scr. Mater. 112 (2016) 118–122.
[13] A.R. Krause, B.S. Senturk, H.F. Garces, G. Dwivedi, A.L. Ortiz, S. Sampath, N.P. Padture, J. Am. Ceram. Soc. 97 (12) (2014) 3943–3949.
[14] A.R. Krause, H.F. Garces, B.S. Senturk, N.P. Padture, J. Am. Ceram. Soc. 97 (12) (2014) 3950–3957.
[15] H.F. Garces, B.S. Senturk, N.P. Padture, Scr. Mater. 76 (2014) 29–32.
[16] J.M. Drexler, A.L. Ortiz, N.P. Padture, Acta Mater. 60 (15) (2012) 5437–5447.
[17] J.M. Drexler, C.H. Chen, A.D. Gledhill, K. Shinoda, S. Sampath, N.P. Padture, Surf. Coat. Technol. 206 (19–20) (2012) 3911–3916.
[18] A.D. Gledhill, K.M. Reddy, J.M. Drexler, K. Shinoda, S. Sampath, N.P. Padture, Mater. Sci. Eng. A Struct. 528 (24) (2011) 7214–7221.
[19] J.M. Drexler, A.D. Gledhill, K. Shinoda, A.L. Vasiliev, K.M. Reddy, S. Sampath, N.P. Padture, Adv. Mater. 23 (21) (2011) 2419–2424.
[20] J.M. Drexler, A. Aygun, D.S. Li, R. Vassen, T. Steinke, N.P. Padture, Surf. Coat. Technol. 204 (16–17) (2010) 2683–2688.
[21] J.M. Drexler, K. Shinoda, A.L. Ortiz, D.S. Li, A.L. Vasiliev, A.D. Gledhill, S. Sampath, N.P. Padture, Acta Mater. 58 (20) (2010) 6835–6844.
[22] E. Bakan, R. Vassen, J. Therm. Spray Technol. 26 (6) (2017) 992–1010.
[23] S. Sampath, U. Schulz, M.O. Jarligo, S. Kuroda, MRS Bull. 37 (10) (2012) 903–910.
[24] X. Shan, Z.H. Zou, L.J. Gu, L.X. Yang, F.W. Guo, X.F. Zhao, P. Xiao, Scr. Mater. 113 (2016) 71–74.
[25] S. Ahmadian, A. Browning, E.H. Jordan, Scr. Mater. 97 (2015) 13–16.
[26] G. Mauer, R. Vassen, Surf. Eng. 27 (7) (2011) 477–479.
[27] W.G. Chi, S. Sampath, H. Wang, J. Am. Ceram. Soc. 91 (8) (2008) 2636–2645.
[28] E. Bakan, D.E. Mack, G. Mauer, R. Mucke, R. Vassen, J. Am. Ceram. Soc. 98 (8) (2015) 2647–2654.
[29] Z. Wang, A. Kulkarni, S. Deshpande, T. Nakamura, H. Herman, Acta Mater. 51 (18) (2003) 5319–5334.
[30] A. Feuerstein, J. Knapp, T. Taylor, A. Ashary, A. Bolcavage, N. Hitchman, J. Therm. Spray Technol. 17 (2) (2008) 199–213.
[31] T.R. Kakuda, A.M. Limarga, T.D. Bennett, D.R. Clarke, Acta Mater. 57 (8) (2009) 2583–2591.
[32] H. Xie, Y.C. Xie, G.J. Yang, C.X. Li, C.J. Li, J. Therm. Spray Technol. 22 (8) (2013) 1328–1336.
[33] G.R. Li, B.W. Lv, G.J. Yang, W.X. Zhang, C.X. Li, C.J. Li, J. Therm. Spray Technol. 24 (8) (2015) 1355–1367.
[34] Y. Tan, J.P. Longtin, S. Sampath, H. Wang, J. Am. Ceram. Soc. 92 (3) (2009) 710–716.
[35] B. Ercan, K.J. Bowman, R.W. Trice, H. Wang, W. Porter, Mater. Sci. Eng. A Struct. 435 (2006) 212–220.
[36] L. Xie, M.R. Dorfman, A. Cipitria, S. Paul, I.O. Golosnoy, T.W. Clyne, J. Therm. Spray Technol. 16 (5–6) (2007) 804–808.
[37] R.E. Taylor, X. Wang, X. Xu, Surf. Coat. Technol. 120 (1999) 89–95.
[38] B.R. Marple, R.S. Lima, C. Moreau, S.E. Kruger, L. Xie, M.R. Dorfman, J. Therm. Spray Technol. 16 (5–6) (2007) 791–797.
[39] S. Paul, A. Cipitria, S.A. Tsipas, T.W. Clyne, Surf. Coat. Technol. 203 (8) (2009) 1069–1074.
[40] A. Cipitria, I.O. Golosnoy, T.W. Clyne, Acta Mater. 57 (4) (2009) 980–992.
[41] S. Paul, A. Cipitria, I.O. Golosnoy, L. Xie, M.R. Dorfman, T.W. Clyne, J. Therm. Spray Technol. 16 (5–6) (2007) 798–803.
[42] F. Cernuschi, P.G. Bison, S. Marinetti, P. Scardi, Acta Mater. 56 (16) (2008) 4477–4488.
[43] F. Cernuschi, L. Lorenzoni, S. Ahmaniemi, P. Vuoristo, T. Mantyla, J. Eur. Ceram. Soc. 25 (4) (2005) 393–400.
[44] R. Dutton, R. Wheeler, K.S. Ravichandran, K. An, J. Therm. Spray Technol. 9 (2) (2000) 204–209.
[45] G.R. Li, H. Xie, G.J. Yang, G. Liu, C.X. Li, C.J. Li, J. Am. Ceram. Soc. 100 (5) (2017) 2176–2189.
[46] A.J. Allen, G.G. Long, H. Boukari, J. Ilavskya, A. Kulkarni, S. Sampath, H. Herman, A.N. Goland, Surf. Coat. Technol. 146 (2001) 544–552.
[47] A.J. Allen, J. Ilavsky, G.G. Long, J.S. Wallace, C.C. Berndt, H. Herman, Acta Mater. 49 (9) (2001) 1661–1675.

[48] S. Kikuchi, M. Tezura, M. Kimura, N. Yamaguchi, S. Kitaoka, T. Kizuka, Scr. Mater. 150 (2018) 50–53.
[49] Y. Yang, Y.F. Cheng, Electrochim. Acta 253 (2017) 134–141.
[50] N. Zidane, Y.A. Albrimi, A.A. Addi, J. Douch, R.M. Souto, M. Hamdani, Int. J. Electrochem. Sci. 13 (1) (2018) 29–44.
[51] A. Osundare, D.T. Oloruntoba, P. Popoola, Anti-Corros. Method. M 65 (2) (2018) 158–165.
[52] N. Markocsan, M. Gupta, S. Joshi, P. Nylen, X.H. Li, J. Wigren, J. Therm. Spray Technol. 26 (6) (2017) 1104–1114.
[53] N.P. Padture, K.W. Schlichting, T. Bhatia, A. Ozturk, B. Cetegen, E.H. Jordan, M. Gell, S. Jiang, T.D. Xiao, P.R. Strutt, E. Garcia, P. Miranzo, M.I. Osendi, Acta Mater. 49 (12) (2001) 2251–2257.
[54] M. Gell, E.H. Jordan, M. Teicholz, B.M. Cetegen, N.P. Padture, L.D. Xie, D.Y. Chen, X.Q. Ma, J. Roth, J. Therm. Spray Technol. 17 (1) (2008) 124–135.
[55] A. Aygun, A.L. Vasiliev, N.P. Padture, X.Q. Ma, Acta Mater. 55 (20) (2007) 6734–6745.
[56] L.D. Xie, E.H. Jordan, N.P. Padture, M. Gell, Mater. Sci. Eng. A Struct. 381 (1–2) (2004) 189–195.
[57] L.D. Xie, X.Q. Ma, E.H. Jordan, N.P. Padture, D.T. Xiao, M. Gell, J. Mater. Sci. 39 (5) (2004) 1639–1646.
[58] A.D. Jadhav, N.P. Padture, Surf. Coat. Technol. 202 (20) (2008) 4976–4979.
[59] M. Gell, L.D. Xie, E.H. Jordan, N.P. Padture, Surf. Coat. Technol. 188 (2004) 101–106.
[60] E.H. Jordan, L. Xie, X. Ma, M. Gell, N.P. Padture, B. Cetegen, A. Ozturk, J. Roth, T.D. Xiao, P.E.C. Bryant, J. Therm. Spray Technol. 13 (1) (2004) 57–65.
[61] M. Gell, L.D. Xie, X.Q. Ma, E.H. Jordan, N.P. Padture, Surf. Coat. Technol. 177 (2004) 97–102.
[62] A. Jadhav, N.P. Padture, F. Wu, E.H. Jordan, M. Gell, Mater. Sci. Eng. A Struct. 405 (1–2) (2005) 313–320.
[63] G. Dwivedi, V. Viswanathan, S. Sampath, A. Shyam, E. Lara-Curzio, J. Am. Ceram. Soc. 97 (9) (2014) 2736–2744.
[64] C.J. Li, Y. Li, G.J. Yang, C.X. Li, J. Therm. Spray Technol. 22 (8) (2013) 1374–1382.
[65] Y. Liu, T. Nakamura, V. Srinivasan, A. Vaidya, A. Gouldstone, S. Sampath, Acta Mater. 55 (14) (2007) 4667–4678.
[66] G.R. Li, H. Xie, G.J. Yang, G. Liu, C.X. Li, C.J. Li, J. Am. Ceram. Soc. 100 (9) (2017) 4240–4251.
[67] K.W. Schlichting, N.P. Padture, E.H. Jordan, M. Gell, Mater. Sci. Eng. A Struct. 342 (1–2) (2003) 120–130.
[68] P. Jiang, X.L. Fan, Y.L. Sun, D.J. Li, B. Li, T.J. Wang, Mater. Des. 132 (2017) 559–566.
[69] P. Jiang, X.L. Fan, Y.L. Sun, D.J. Li, T.J. Wang, Int. J. Solids Struct. 130 (2018) 11–20.
[70] N. Wang, C.N. Zhou, S.K. Gong, H.B. Xu, Ceram. Int. 33 (6) (2007) 1075–1081.
[71] G.R. Li, G.J. Yang, C.X. Li, C.J. Li, Ceram. Int. 43 (13) (2017) 9600–9615.
[72] G.R. Li, G.J. Yang, C.X. Li, C.J. Li, J. Eur. Ceram. Soc. 38 (9) (2018) 3326–3332.
[73] K.A. Erk, C. Deschaseaux, R.W. Trice, J. Am. Ceram. Soc. 89 (5) (2006) 1673–1678.
[74] A.J. Shaler, H. Udin, G.C. Kuczynski, M. Bever, T. Am. I. Min. Met. Eng. 185 (11) (1949) 896–897.
[75] A.D. Jadhav, N.P. Padture, E.H. Jordan, M. Gell, P. Miranzo, E.R. Fuller, Acta Mater. 54 (12) (2006) 3343–3349.
[76] T. Liu, X.T. Luo, X. Chen, G.J. Yang, C.X. Li, C.J. Li, J. Therm. Spray Technol. 24 (5) (2015) 739–748.
[77] I.O. Golosnoy, S.A. Tsipas, T.W. Clyne, J. Therm. Spray Technol. 14 (2) (2005) 205–214.
[78] I.O. Golosnoy, A. Cipitria, T.W. Clyne, J. Therm. Spray Technol. 18 (5–6) (2009) 809–821.